Hydrodynamic approach to the interaction of a relativistic ultrashort laser pulse with an underdense plasma

Daniela Farina and Maurizio Lontano
Istituto di Fisica del Plasma, CNR, 20125 Milan, Italy

Ivane G. Murusidze and Solomon V. Mikeladze
Institute of Physics, Georgian Academy of Sciences, 380077 Tbilisi, Georgia
(Received 14 December 2000; published 26 April 2001)

The interaction of an ultrashort, high peak power laser pulse with an underdense plasma is investigated within a physical model based on the three-dimensional cold hydrodynamic approach, which allows one to study the dynamics of the laser pulse and of the generated wakefields self-consistently, in the fully relativistic, strongly nonlinear regime. Our model is developed with the aim of describing very short laser pulses (with $\ell_0 < \lambda_p$ and $\ell_0 \ll \ell_\perp$, where $\ell_0, \ell_\perp, \lambda_p$ are the pulse length, its transverse scale, and the plasma wavelength, respectively) down to single cycle radiation wave packets, which have become available with the recent progress in laser technology. The space-time structure and the evolution of large quasistatic electric and magnetic fields are studied, together with the pulse dynamics, by the direct numerical integration of the relativistic fluid and field equations, within the extended paraxial approximation.

DOI: 10.1103/PhysRevE.63.056409 PACS number(s): 52.38.−r, 52.35.Mw, 52.40.Db

I. INTRODUCTION

Advances in laser technology, based mainly on the technique of chirped-pulse amplification (CPA) [1], enable one to produce high-intensity (in excess of 10^{18} W/cm^2) high peak-power (from multiterawatt to petawatt) laser pulses [2,3]. Petawatt peak powers are exceeded in large systems producing kilojoule-class subpicosecond (≈ 450 fs) pulses [2,4]. Further progress in the development of tabletop multiterawatt, ultrashort-pulse systems has made it possible to generate sub-30-femtosecond laser pulses with peak power in excess of 40 TW [5]. CPA technology has allowed the construction of a compact laser system generating pulses with peak powers in excess of 100 TW and durations of less than 19 fs [6]. The same technique can be used to develop a laboratory-scale laser system producing ≈ 20 fs laser pulses with 1 PW peak power. In these systems, the output intensities reach 10^{19} W/cm^2, whereas focused intensities available with such pulses are in the $10^{20}-10^{21}$ W/cm^2 range. At these intensities, the electron motion in the laser fields becomes highly nonlinear and relativistic, and a completely new field of nonlinear physics, characterized by the extreme physical conditions of the target plasma, has become the subject of laboratory investigations in recent years.

The interaction of high-intensity, ultrashort laser pulses with an underdense plasma is of primary interest for laser-plasma particle accelerators, laser-induced x-ray lasers, and many other envisaged applications [7]. This is a topic of considerable interest even for the fast ignitor concept of the inertial confinement fusion [8]. Although its ultimate goal is the penetration of a short, bright laser pulse in the overdense core, before reaching it the pulse has to travel a considerable distance through the underdense corona.

An issue of particular concern, when investigating the relativistically intense laser-plasma interaction, is the generation of a multimegagauss quasistatic magnetic field behind the laser pulse. This process deserves particular interest both from the point of view of diagnostics and for the role played by such a huge magnetic field when electron bunches should be introduced into the accelerating region of a plasma-based laser wakefield accelerator. Recently, a number of analytical studies [9,11] and numerical [particle-in-cell (pic)] simulations [9,10,12–17] have demonstrated that a relativistically intense laser pulse produces a quasistatic magnetic wake behind itself, associated with the currents of fast electrons, which are produced due to several mechanisms: the accelerating longitudinal electrostatic field, the relativistic ponderomotive forces, and the wavebreaking of the wakefield.

Research in the plasma-based acceleration of charged particles stimulated the studies of large-amplitude relativistic wakefields generated by a laser pulse. In addition, the relativistic and ponderomotive self-focusing and the optical guiding of intense laser beams in plasmas have been the topics of intense studies, too [18,19].

These works mainly deal with laser pulses in the picosecond and subpicosecond (hundreds of femtoseconds) time range with a typical transverse dimension of a few micrometers. The hydrodynamic approach to the propagation and the nonlinear interaction of these relatively long and narrow pulses with underdense, cold plasmas has proved to be fruitful. For example, the relativistic and ponderomotive self-focusing, various other instabilities, such as envelope modulations, hosing, etc., have been discovered and studied within the fluid model. Relevant theoretical analyses are usually based on the paraxial wave equation containing the diffraction and nonlinear refraction terms, but neglecting the finite pulse duration effects as well as Raman-type instabilities. Therefore, they do not describe the temporal evolution of the pulse due to dispersion effects. This approach is valid for long laser pulses or laser beams. Indeed, in these cases the dispersion effects are insignificant unless $\ell_0/\ell_\perp \approx \omega_p/\omega$, i.e., in underdense plasmas [$\omega_p/\omega \ll 1$, $\omega_p = (4\pi n_0 e^2/m)^{1/2}$ being the plasma frequency] they can be neglected for pulses

with lengths longer than their widths.

In this paper, we study sub-20-femtosecond relativistic laser pulses propagating in an underdense plasma. For these pulses with $\ell_0 \ll \ell_\perp$, the dispersion plays as important a role as the diffraction. It should be noted also that if the pulse duration is on a femtosecond time scale, i.e., $\approx 10-20$ fs for $\lambda \approx 1$ μm radiation, it will contain only a few optical cycles, which makes it necessary to take into account also first-order dispersion effects. Furthermore, often these pulses are so short that $\ell_0 < \lambda_p$, where λ_p is the plasma wavelength, i.e., these pulses do not see even a single plasma wavelength. Therefore, their coupling with plasma waves cannot be described in terms of wave-wave interactions. The shortness of the pulse can suppress parametric Raman processes and significantly limit the number of instabilities. However, an ultrashort pulse experiences new types of instability.

Two aspects in the physics of the laser-plasma interactions can be identified: first, the propagation and the evolution of the laser pulse itself; second, the plasma response to the laser radiation, though in the nonlinear regimes these two aspects cannot be treated separately. However, depending on the particular problem at hand, one of the two is emphasized.

Here, an adequate physical model of the propagation of an ultrashort, ultraintense laser pulse in an underdense plasma is developed. We formulate the so-called pulsed paraxial wave equation (PPWE), which extends the conventional paraxial wave equation systematically, incorporating all possible finite-pulse-length effects. With the group velocity dispersion (GVD) and the first-order dispersion terms retained, the PPWE is applicable to a wide range of ultarshort laser pulses including single cycle pulses. The equations describing the dynamical plasma response to such short pulses complete the set of coupled equations that gives a fully relativistic formulation of the propagation of ultrashort ultrabright laser pulses in underdense plasmas.

Specifically, we consider the interaction of a strong circularly polarized ultrashort ($\ell_0 < \lambda_p$) laser pulse with an underdense ($\omega_p/\omega \ll 1$) plasma, on the basis of a three-dimensional hydrodynamic model. In Sec. II, the physical model is outlined and a short discussion of the ''sources'' of the magnetic field is presented. The *extended paraxial approximation* is introduced in Sec. III, where the validity limits of our model are given. The reduction of the relevant system of equations for a strongly underdense plasma is carried out in Sec. IV. In particular, Sec. IV contains the equations for the coupled evolution of the laser pulse and of the electromagnetic wakefield produced in the plasma. The numerical results are presented and discussed in Sec. V. Section VI is devoted to concluding remarks.

II. PHYSICAL MODEL

Within the hydrodynamic model, the equations describing the laser-plasma interaction can be written in terms of the vector and scalar potentials, $\boldsymbol{A}, \phi$, of the electron momentum $\boldsymbol{p}$, and density n, as

$$\Delta \boldsymbol{A} - \frac{1}{c^2}\frac{\partial^2 \boldsymbol{A}}{\partial t^2} = \frac{4\pi e}{mc}\frac{n\boldsymbol{p}}{\gamma} + \frac{1}{c}\frac{\partial \nabla \phi}{\partial t}, \tag{1}$$

$$\nabla^2 \phi = 4\pi e(n - n_0), \tag{2}$$

$$\frac{\partial \boldsymbol{p}}{\partial t} = \frac{e}{c}\frac{\partial \boldsymbol{A}}{\partial t} + \frac{\boldsymbol{p}}{\gamma} \times \left[\nabla \times \left(\boldsymbol{p} - \frac{e}{c}\boldsymbol{A}\right)\right] + \nabla(e\phi - mc^2\gamma), \tag{3}$$

$$\frac{\partial n}{\partial t} + \nabla \cdot \left(\frac{n\boldsymbol{p}}{m\gamma}\right) = 0. \tag{4}$$

Here, $\gamma = \sqrt{1 + p^2/m^2c^2}$ is the relativistic factor and n_0 is the background density. The Coulomb gauge, $\nabla \cdot \boldsymbol{A} = 0$, has been used.

The electron momentum equation (3) can be cast in the convenient form

$$\frac{\partial \boldsymbol{\Omega}}{\partial t} = \nabla \times (\boldsymbol{v} \times \boldsymbol{\Omega}), \tag{5}$$

which shows that the generalized electron vorticity, $\boldsymbol{\Omega} = \nabla \times \boldsymbol{P}$, is frozen into the electron fluid. Here, $\boldsymbol{P} = \boldsymbol{p} - (e/c)\boldsymbol{A}$ is the canonical electron momentum and $\boldsymbol{v} = \boldsymbol{p}/m\gamma$ is the electron velocity. If initially, at $t = 0$, the electrons are at rest and the laser field is absent, that is, $\boldsymbol{P} = 0$, then Eq. (3) states that $\nabla \times [\boldsymbol{p} - (e/c)\boldsymbol{A}] = \boldsymbol{0}$ holds all along the subsequent interaction, that is, $\boldsymbol{B} = (c/e)\nabla \times \boldsymbol{p}$. Applying the *curl* operator to Eq. (1), we derive the equation governing the magnetic field in the laser-plasma interaction:

$$\Delta \boldsymbol{B} - \frac{1}{c^2}\frac{\partial^2 \boldsymbol{B}}{\partial t^2} - \frac{\omega_p^2}{c^2}\frac{n}{n_0\gamma}\boldsymbol{B} = -\frac{4\pi e}{mc}\boldsymbol{p} \times \nabla \frac{n}{\gamma} = \boldsymbol{S}. \tag{6}$$

Equation (6) is a general equation for the magnetic field involved in such an interaction, which describes both the laser magnetic field and the magnetic field induced in the plasma by the laser pulse itself. The magnetic field is nonlinearly coupled to the electron dynamics through the last term on the left-hand side and the right-hand side of Eq. (6). In view of the forthcoming reduction of Eqs. (1)–(4) under the assumption of underdense plasma, it may be worth separating explicitly the contribution to the source term due to the ''parallel'' (along the propagation direction of the laser pulse) momentum, i.e.,

$$\boldsymbol{S}_{p_z} = -\frac{4\pi e}{mc} p_z \left(\hat{\boldsymbol{e}}_\theta \frac{\partial}{\partial r} - \hat{\boldsymbol{e}}_r \frac{1}{r}\frac{\partial}{\partial \theta}\right)\frac{n}{\gamma}, \tag{7}$$

from that due to the ''transverse'' motion of the electrons, which reads

$$\boldsymbol{S}_{p_\perp} = -\frac{4\pi e}{mc}\left[\hat{\boldsymbol{e}}_z\left(p_r \frac{1}{r}\frac{\partial}{\partial \theta} - p_\theta \frac{\partial}{\partial r}\right) + (\hat{\boldsymbol{e}}_r p_\theta - \hat{\boldsymbol{e}}_\theta p_r)\frac{\partial}{\partial z}\right]\frac{n}{\gamma}. \tag{8}$$

Provided the laser pulse itself can be identified as a driver with a well-localized electromagnetic structure, though evolving in time and space, then the right-hand side of Eq. (6) can be treated as a source ($\boldsymbol{S}$) for the magnetic fields driven by the laser pulse. Supposing that this requirement is met (which will be a matter of deeper investigation in the continuation of this paper), we can discuss the physical

meaning and some ''topological'' features of the right-hand side of Eq. (6) as a source for the laser-driven magnetic fields before making any specific assumption about the laser pulse characteristics or introducing any particular model of the laser-plasma interaction.

First, notice that, according to Eq. (6), a nonvanishing source term implies the space inhomogeneity of the particle density and of the electron mass, or at least of one of the two. However, this is just a necessary condition to form a nonzero source. It is also necessary that the corresponding gradients of plasma parameters form a nonzero vector product with the momentum of plasma electrons. From the expression of the source term, it is obvious that the source and the corresponding magnetic field are always polarized in the plane perpendicular to that formed by the electron momentum and the plasma gradients. Moreover, it should be noticed that, generally speaking, both the momentum of the electrons in the laser-excited wakefield and the momentum acquired by the electrons inside the laser field contribute to the source term. In the latter case, the source is localized within the pulse region. Depending on the polarization of the laser and on the particular geometry of the problem, rapidly oscillating (on the laser period time scales) magnetic fields, as well as ''quasistatic'' magnetic fields, varying on time scales of the order of the plasma frequency or its harmonics, may be generated. Inside the region occupied by the laser pulse, magnetic-field generation is possible even in a one-dimensional geometry, while behind the pulse, where the n's and p's in the source term are related to the laser-excited wakefield, at least a two-dimensional geometry is required to have a nonvanishing source.

In order to easily identify the order of magnitude of the terms appearing in Eqs. (1)–(4), which govern the laser-plasma interaction, it is worth introducing suitable dimensionless variables. Let $\ell_\parallel$ be the characteristic distance over which the laser pulse shape changes appreciably, $\ell_\perp$ the typical transverse (to the propagation direction) scale of the laser pulse, $\ell_0=\tau_0 v_g$ the laser pulse length, where τ_0 is its time duration, and v_g the laser group velocity. Then, we can go to the reference frame comoving with the laser pulse, and introduce the following transformations of variables: $z/\ell_\parallel \rightarrow \zeta$, $\boldsymbol{r}_\perp/\ell_\perp \rightarrow \boldsymbol{r}$, $(t-z/v_g)/\tau_0 \rightarrow \tau$, $\boldsymbol{p}/mc \rightarrow \boldsymbol{p}$, $e\phi(\boldsymbol{A})/mc^2 \rightarrow \phi(\boldsymbol{A})$, $e\boldsymbol{E}(\boldsymbol{B})/mc\omega_p \rightarrow \boldsymbol{E}(\boldsymbol{B})$, $n/n_0 \rightarrow n$.

In terms of the normalized variables, the hydrodynamic Eqs. (3) and (4) take the form

$$\frac{\partial \boldsymbol{p}_\perp}{\partial \tau}=\frac{\partial \boldsymbol{A}_\perp}{\partial \tau}+\frac{\ell_0/\ell_\perp}{\beta_g}\boldsymbol{\nabla}_\perp(\phi-\gamma), \tag{9}$$

$$\frac{\partial p_z}{\partial \tau}=\frac{\partial A_z}{\partial \tau}-\frac{1}{\beta_g}\frac{\partial}{\partial \tau}(\phi-\gamma)+\frac{\ell_0/\ell_\parallel}{\beta_g}\frac{\partial}{\partial \zeta}(\phi-\gamma), \tag{10}$$

$$\frac{\partial n}{\partial \tau}-\frac{1}{\beta_g}\frac{\partial}{\partial \tau}\left(\frac{np_z}{\gamma}\right)+\frac{\ell_0/\ell_\parallel}{\beta_g}\frac{\partial}{\partial \zeta}\left(\frac{np_z}{\gamma}\right)+\frac{\ell_0/\ell_\perp}{\beta_g}\boldsymbol{\nabla}_\perp\cdot\left(\frac{n\boldsymbol{p}_\perp}{\gamma}\right)=0. \tag{11}$$

Then, the field Eqs. (1) and (2) read

$$\left[(1-\beta_g^2)\frac{\partial^2}{\partial \tau^2}-2\frac{\ell_0}{\ell_\parallel}\frac{\partial^2}{\partial \tau \partial \zeta}+\left(\frac{\ell_0}{\ell_\perp}\right)^2\boldsymbol{\nabla}_\perp^2+\left(\frac{\ell_0}{\ell_\parallel}\right)^2\frac{\partial^2}{\partial \zeta^2}\right]\boldsymbol{A}=(k_p\ell_0)^2\frac{n}{\gamma}\boldsymbol{p}+\beta_g\frac{\partial}{\partial \tau}\left[\hat{\boldsymbol{e}}_z\left(\frac{\ell_0}{\ell_\parallel}\frac{\partial}{\partial \zeta}-\frac{\partial}{\partial \tau}\right)\phi+\frac{\ell_0}{\ell_\perp}\boldsymbol{\nabla}_\perp\phi\right], \tag{12}$$

$$\frac{\partial^2\phi}{\partial \tau^2}-2\frac{\ell_0}{\ell_\parallel}\frac{\partial^2\phi}{\partial \tau \partial \zeta}+\left(\frac{\ell_0}{\ell_\perp}\right)^2\boldsymbol{\nabla}_\perp^2\phi+\left(\frac{\ell_0}{\ell_\parallel}\right)^2\frac{\partial^2\phi}{\partial \zeta^2}=(k_p\ell_0)^2(n-1), \tag{13}$$

where we have introduced $\beta_g=v_g/c$ and $k_p=\sqrt{4\pi n_0 e^2/mc^2}$.

Equations (9)–(13) are exact. The various terms occurring in the above equations are weighted by the dimensionless quantities 1, $\ell_0/\ell_\perp$, $\ell_0/\ell_\parallel$, sometimes occurring to the second power. In the next section, we shall use these weighting factors to exploit the *extended paraxial approximation*.

III. THE EXTENDED PARAXIAL APPROXIMATION

Let us assume that the vector potential is circularly polarized in its transverse component, that is,

$$\boldsymbol{A}(\boldsymbol{r}_\perp,z,t)=\tfrac{1}{2}\{[(\hat{\boldsymbol{e}}_x+i\hat{\boldsymbol{e}}_y)A(\boldsymbol{r}_\perp,z,t)+\hat{\boldsymbol{e}}_z A_z(\boldsymbol{r}_\perp,z,t)]\times e^{ikz-i\omega t}+\text{c.c.}\}, \tag{14}$$

where A and A_z are complex functions. By substituting Eq. (14) into Eq. (12), we obtain the following equation for the complex amplitude of the transverse component of the vector potential:

$$\begin{aligned}2ik\ell_0\frac{\ell_0}{\ell_\parallel}\frac{\partial A}{\partial \zeta}-2\frac{\ell_0}{\ell_\parallel}\frac{\partial^2 A}{\partial \zeta \partial \tau}+\left(\frac{\ell_0}{\ell_\perp}\right)^2\nabla_\perp^2 A&+\mathcal{D}\frac{\partial^2 A}{\partial \tau^2}+\left(\frac{\ell_0}{\ell_\parallel}\right)^2\frac{\partial^2 A}{\partial \zeta^2}\\&=(k_p\ell_0)^2\left(\frac{n}{\gamma}-1\right)A+\frac{\ell_0}{\ell_\perp}\left[(k_p\ell_0)^2\frac{1}{\beta_g}\frac{n}{\gamma}\right.\\&\left.\times\int^\tau d\tau'\boldsymbol{\nabla}_{xy}(\phi-\gamma)+\beta_g\frac{\partial(\nabla_{xy}\phi)}{\partial \tau}\right]\\&\times\exp\left[i\omega\tau_0\left(\tau+\frac{\ell_\parallel}{\ell_0}\frac{\omega_p^2}{\omega^2}\zeta\right)\right].\end{aligned} \tag{15}$$

Here, $\mathcal{D}$ is related to the GVD by $\mathcal{D}\equiv -v_g^2 k\partial^2 k/\partial\omega^2=\omega_p^2/\omega^2$. Moreover, in writing Eq. (15), the first-order differential operator $\boldsymbol{\nabla}_{xy}=\partial/\partial x-i\partial/\partial y$ has been introduced.

In order to simplify Eq. (15), though retaining a widely applicable formulation of the problem, let us assume that the first four terms on the left-hand side may be of the same order during the space-time evolution of the laser-plasma system. Physically, the third and the fourth terms on the left-hand side represent the diffraction of the pulse, due to its finite transverse extension, and the GVD, weighted by the ratio ω_p^2/ω^2, respectively. By assuming that these two terms

remain of the same order, then for an ultrashort laser pulse (where its length is much shorter than its width) propagating in a strongly underdense plasma, we can introduce the ''natural'' smallness parameter $\ell_0^2/\ell_\perp^2 \approx \omega_p^2/\omega^2 = \epsilon^2 \ll 1$.

A further independent smallness parameter occurs in the problem, that is, $\nu = (k\ell_\parallel)^{-1} \ll 1$. By assuming that the first two terms are of the same order as the third and the fourth, we obtain that $\nu \sim \epsilon^2$. Then, the following scalings hold:

$$\ell_0/\ell_\perp \sim \ell_\perp/\ell_\parallel \sim \omega_p/\omega = \epsilon$$

and

$$\ell_0/\ell_\parallel \sim \lambda/\ell_\parallel \sim \epsilon^2.$$

The above scalings can then be used to simplify the equations. In particular, on the left-hand side of Eq. (15), the last term (of order ϵ^2) can be neglected with respect to the others (of order ϵ). Physically, it corresponds to assuming that it takes a long path of propagation to modify appreciably the laser pulse shape. The remaining terms describe a wide class of effects: the first term gives the propagation at the group velocity, the second term allows us to extend the applicability of our model to very short laser pulses, even to single-cycle pulses. In the next section, we shall use the ''natural'' ordering suggested by the left-hand side of Eq. (15) to expand the system of Eqs. (9)–(13) in order to describe the propagation of an ultrashort relativistic laser pulse into an underdense plasma.

IV. THE REDUCTION OF THE EQUATIONS TO THE CASE OF AN UNDERDENSE PLASMA

The structure on the left-hand side of Eq. (15) suggests introducing the following expansion for all the physical quantities:

$$\boldsymbol{Q} = \boldsymbol{Q}_0 + \boldsymbol{Q}_1 + \cdots, \quad A_z = A_{z,1} + \cdots, \tag{16}$$

where $\boldsymbol{Q} \to \boldsymbol{p}_\perp, \boldsymbol{A}_\perp, p_z, \gamma, n$. The leading-order term $\boldsymbol{A}_{\perp,0}$ represents the laser field. It is worth noticing that the expansion of Eq. (16) does not imply any weakly relativistic approximation.

A. The zeroth-order equations ($\epsilon = 0$)

In the limit $\epsilon \to 0$, the zeroth-order hydrodynamic equations for the transverse and the longitudinal components of the electron momentum and the continuity equation read, respectively,

$$\frac{\partial \boldsymbol{p}_{\perp,0}}{\partial \tau} = \frac{\partial \boldsymbol{A}_{\perp,0}}{\partial \tau}, \tag{17}$$

$$\frac{\partial p_{z,0}}{\partial \tau} = -\frac{1}{\beta_g}\frac{\partial}{\partial \tau}(\phi_0 - \gamma_0), \tag{18}$$

$$\frac{\partial n_0}{\partial \tau} - \frac{1}{\beta_g}\frac{\partial}{\partial \tau}\left(\frac{n_0 p_{z,0}}{\gamma_0}\right) = 0. \tag{19}$$

Upon integration, the above equations read

$$\boldsymbol{p}_{\perp,0} = \boldsymbol{A}_{\perp,0}, \tag{20}$$

$$\beta_g p_{z,0} = -(\phi_0 - \gamma_0) - 1, \tag{21}$$

$$(\beta_g - p_{z,0}/\gamma_0) n_0 = \beta_g. \tag{22}$$

The zeroth-order field equations read

$$A_{z,0} = 0, \tag{23}$$

$$\Box^2 A_0 + 2ik\ell_0 \frac{\ell_0}{\ell_\parallel}\frac{\partial A_0}{\partial \zeta} = (k_p \ell_0)^2 \left\{ \frac{\beta_g}{[(1+\phi_0)^2 - \gamma_{\perp,0}^2/\gamma_g^2]^{1/2}} - 1 \right\} A_0, \tag{24}$$

$$\frac{\partial^2 \phi_0}{\partial \tau^2} = (k_p \ell_0)^2 \gamma_g^2 \left\{ \frac{\beta_g (1+\phi_0)}{[(1+\phi_0)^2 - \gamma_{\perp,0}^2/\gamma_g^2]^{1/2}} - 1 \right\}. \tag{25}$$

In the above equations, we have defined $\gamma_0 = (1 + p_{z,0}^2 + |A_0|^2)^{1/2}$, $\gamma_{\perp,0} = (1 + |A_0|^2)^{1/2}$, and $\gamma_g = (1 - \beta_g^2)^{-1/2}$, and introduced the following second-order differential operator:

$$\Box^2 \equiv \left(\frac{\ell_0}{\ell_\perp}\right)^2 \nabla_\perp^2 - 2\frac{\ell_0}{\ell_\parallel}\frac{\partial^2}{\partial \tau \partial \zeta} + \frac{\omega_p^2}{\omega^2}\frac{\partial^2}{\partial \tau^2}. \tag{26}$$

It is important to note that Eq. (24) is no longer a parabolic equation. The right name for it, according to its content, would be the *pulsed paraxial wave equation*. The hierarchy of scales implied by this equation naturally leads to the plasma response, which is self-consistently described within the *quasistatic approximation*.

B. The first-order equations ($\epsilon \ll 1$)

The first-order hydrodynamic equations read

$$\frac{\partial \boldsymbol{p}_{\perp,1}}{\partial \tau} = \frac{\partial \boldsymbol{A}_{\perp,1}}{\partial \tau} + \frac{\epsilon}{\beta_g}\boldsymbol{\nabla}_\perp(\phi_0 - \gamma_0), \tag{27}$$

$$\frac{\partial p_{z,1}}{\partial \tau} = \frac{\partial A_{z,1}}{\partial \tau} - \frac{1}{\beta_g}\frac{\partial}{\partial \tau}(\phi_1 - \gamma_1), \tag{28}$$

$$\frac{\partial n_1}{\partial \tau} - \frac{1}{\beta_g}\frac{\partial}{\partial \tau}\left[\frac{n_1}{\gamma_0}p_{z,0} + \frac{n_0}{\gamma_0}p_{z,1} - \frac{n_0}{\gamma_0^2}p_{z,0}\gamma_1\right] + \frac{\epsilon}{\beta_g}\nabla_\perp \cdot \left(\frac{\boldsymbol{p}_{\perp,0}}{\gamma_0}n_0\right) = 0, \tag{29}$$

where $\gamma_1 = (\boldsymbol{p}_{\perp,0}\cdot\boldsymbol{p}_{\perp,1} + p_{z,0}p_{z,1})/\gamma_0$.

The first-order field equations read

$$\Box^2 A_{z,1} = (k_p \ell_0)^2 \left[\frac{n_1}{\gamma_0}p_{z,0} + \frac{n_0}{\gamma_0}p_{z,1} - \frac{n_0}{\gamma_0^2}p_{z,0}\gamma_1\right] - \beta_g \frac{\partial^2 \phi_1}{\partial \tau^2}, \tag{30}$$

$$\Box^2 \boldsymbol{A}_{\perp,1} = (k_p \ell_0)^2 \left[\frac{n_1}{\gamma_0} \boldsymbol{p}_{\perp,0} + \frac{n_0}{\gamma_0} \boldsymbol{p}_{\perp,1} - \frac{n_0}{\gamma_0^2} \boldsymbol{p}_{\perp,0} \gamma_1 \right] + \beta_g \frac{\ell_0}{\ell_\perp} \frac{\partial}{\partial \tau} (\boldsymbol{\nabla}_\perp \phi_0), \tag{31}$$

$$\frac{\partial^2 \phi_1}{\partial \tau^2} = (k_p \ell_0)^2 n_1 . \tag{32}$$

Equations (27)–(32), together with Eqs. (20)–(25), completely describe the laser-plasma interaction within the extended paraxial approximation in an underdense plasma. We observe that the procedure outlined in the previous sections actually separates the evolution of the laser magnetic field [at the zeroth order, see Eq. (24)] from the evolution of the induced quasistatic magnetic field [at the first order, see Eqs. (30) and (31)].

V. NUMERICAL SIMULATIONS

We have integrated the system of Eqs. (27)–(32), coupled with Eqs. (20)–(25), for circularly polarized laser pulses, of relativistic amplitudes ($A \geqslant 1$). A finite-difference numerical scheme is used, with first-order accuracy in ζ and second-order accuracy in x, y, r, and τ. The boundary conditions are of ''radiating'' type, with neither reflection nor absorption. The simulations presented in this section model the interaction of an ultrashort, relativistically intense, high-power laser pulse with a plasma. Initially, the laser pulse is focused at the edge of a preformed underdense plasma, with $n/n_{\rm cr}=0.01$ (corresponding to $\omega_p/\omega=0.1$), where $n_{\rm cr}$ is the critical plasma density. At the input (edge) plane, the electromagnetic field distribution is given by $A = a_0 \exp(-\tau^2/\tau_0^2 - r^2/w_0^2)$, where $r=(x^2+y^2)^{1/2}$. This axially symmetric distribution, with Gaussian transverse and longitudinal profiles, corresponds to the fundamental Gaussian mode with a spot size w_0 and a planar wavefront at the input plane. The axial symmetry is maintained during the entire time evolution of the system. The initial effective pulse duration, τ_0, is related to the spot size by the relationship $v_g \tau_0 / w_0 = 0.1$. Other relevant dimensionless parameters in our simulations are the ratio of the laser spot size to the plasma skin depth, $k_p w_0 = 25$, and $k_p Z_R = 3125$, where Z_R is the vacuum Rayleigh length.

Here, we present the numerical results relevant to the cases with $a_0=1$ and $a_0=3$ for an unperturbed cold plasma characterized by the electron density $n_e = 9.9\times 10^{18}$ cm^{-3} corresponding to a plasma wavelength of $\lambda_p = 2\pi/k_p = 10.6$ μm. With this last choice, the normalized electric and magnetic fields are referred to the following unitary values:

$$\frac{mc\omega_p}{e} \approx 3.03\times 10^9 \frac{\rm V}{\rm cm}, \quad \frac{mc\omega_p}{e} \approx 1.01\times 10^7 \ \ {\rm G},$$

respectively. The laser pulse is characterized by the following unperturbed parameters: vacuum wavelength $\lambda = 1.06$ μm; full length at half maximum $\ell_{\rm FWHM} = 5(4.2)$ μm, corresponding to a time duration of $\tau_0 = 16.7$ (14.1) fs; peak power $P_0 = 614$ (68) TW; peak intensity $I_0 = 2.2\times 10^{19}$ (2.4×10^{18}) W/cm^2; for $a_0=3$ (1). The Rayleigh length in vacuum is $Z_R = 5272$ μm and the initial waist is $w_0 = 42$ μm, in both cases.

Figure 1 shows the contour plots of the longitudinal electrostatic field, E_z [Fig. 1(a)], of the electron density, n [Fig. 1(b)], and of the longitudinal electron momentum, p_z [Fig. 1(c)], associated with the wakefield produced behind the laser pulse (which is localized around $z'=0$), in the plane ($r'=k_p r, z' = -k_p(z - v_g t)$, taken after traveling $z = 52.5$ μm (left column) and $z = 316.1$ μm (right column) from the input plane ($z=0$), for $a_0=3$. We remind the reader that at $z=0$, the pulse scales are $k_p w_0 = 25$ and $k_p v_g \tau_0 = 2.5$. In Fig. 1(a) we see that already at the very beginning of the interaction (left column) the dynamics is intrinsically nonlinear, i.e., the front of the wakefield is strongly curved towards the pulse and the maximum accelerating field has reached a value of ≈ 0.5 TV/m. This value is then bound to further increase during the pulse propagation (right column) due to the evolution of the pulse itself. Figure 1(b) displays the contour plots of the electron density at the same z positions as in Fig. 1(a). The strong spiky structure of the density is evident, although the wavebreaking conditions are not yet achieved even at $z = 316.1$ μm. Finally, Fig. 1(c) shows the contour plots of the parallel electron momentum from which we get the fully relativistic character of the dynamic, with $|p_{z,\rm max}| \approx 4.3$. E_z, n, p_z are zeroth-order quantities, in our model (in Sec. IV A they have a 0 index). From our simulations, such quantities manifest a spatial periodicity that is approximately of $11 k_p^{-1} \approx 1.75 \lambda_p$ at $z = 316.1$ μm, and it increases with increasing laser intensity. Notice that the scale of such a periodicity is much longer than that usually argued on the basis of the generation of the second spatial harmonic of the background plasma wave vector, even if the relativistic mass correction is considered. Indeed, in our case the circular polarization of the laser prevents the occurrence of harmonics of the laser.

It is worth observing that the strong curvature of the wavefronts, which occurs during the pulse propagation, is a combined effect of the relativistic electron mass dependence on the particle velocity and of the spiky structure of the electron density. It is known [20,21] that in one-dimensional (1D) geometry, for a given laser pulse, its group velocity equals the phase velocity of the electrostatic oscillation induced behind itself. By extrapolating this property to the 3D case, where $\ell_0 \ll \ell_\perp$ and $\ell_0 \ll \ell_\parallel$, i.e., taking

$$v_g \approx c \left(1 - \frac{\omega_{p,\rm NL}^2}{\omega^2} \right)^{1/2} = c \left(1 - \frac{\omega_p^2}{\omega^2} \frac{n}{\gamma} \right)^{1/2},$$

by varying it, we get

$$\delta v_g \approx \frac{c^2}{2 v_g} \frac{\omega_{p,\rm NL}^2}{\omega^2} \left(\frac{\delta \gamma}{\gamma} - \frac{\delta n}{n} \right), \tag{33}$$

where $\omega_{p,\rm NL} = \sqrt{4\pi n e^2 / m\gamma}$ is the nonlinear electron plasma frequency. Here, both $\gamma = \sqrt{1 + p_z^2 + p_\perp^2}$ and n behave nonlin-

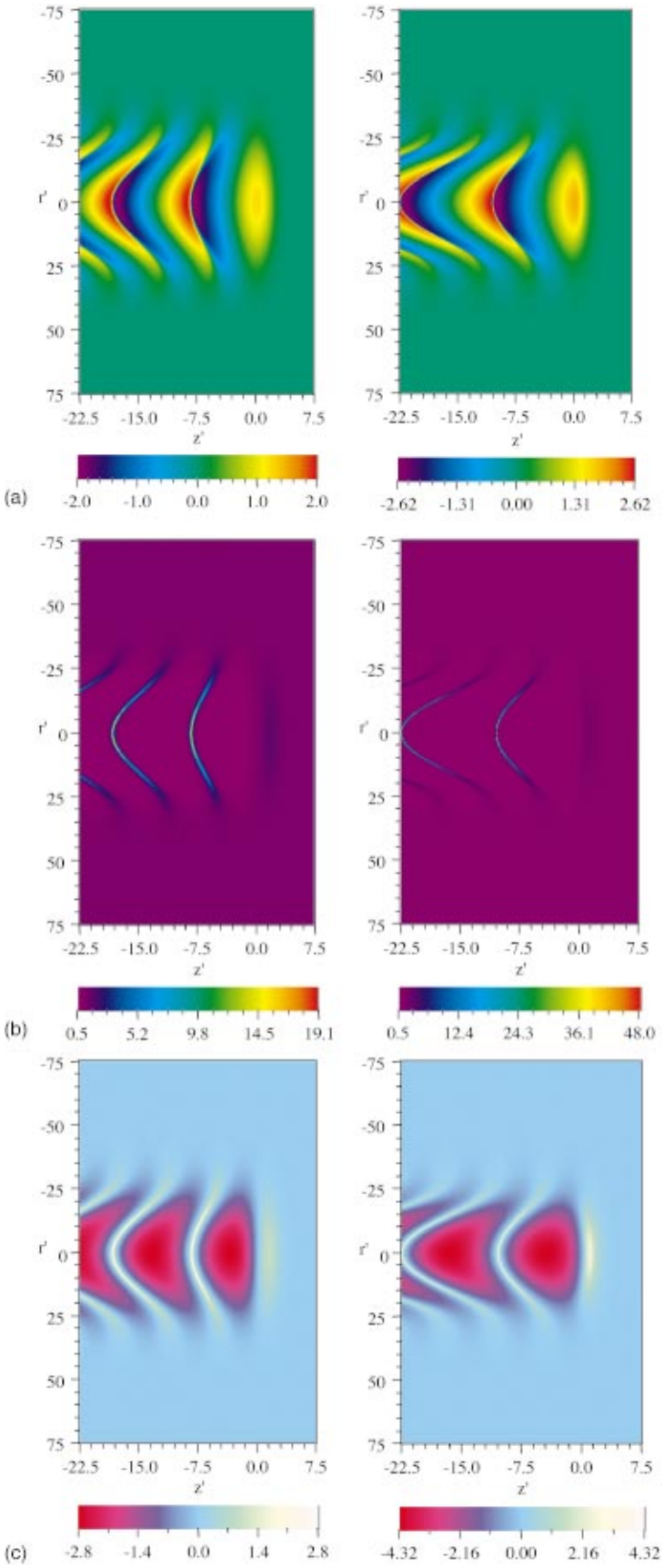

FIG. 1. (Color) The contour plots of the longitudinal electrostatic field E_z (a), of the electron density n (b), and of the longitudinal electron momentum p_z (c), associated with the wakefield produced behind the laser pulse (localized around $z'=0$), in the plane $(r'=k_p r, z'=-k_p(z-v_g t)$, are shown taken after traveling $z=52.5$ μm (left column) and $z=316.1$ μm (right column) from the input plane $(z=0)$ for $a_0=3$.

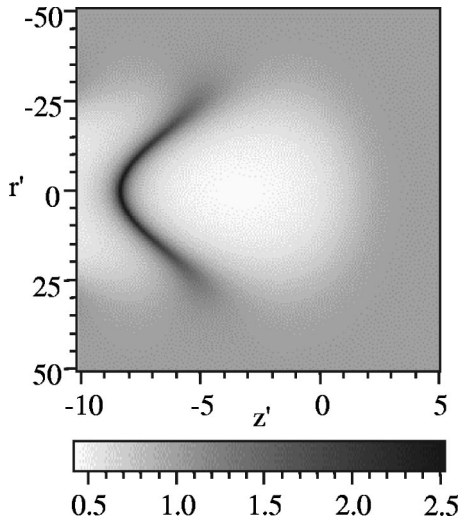

FIG. 2. The surface plot of $\omega_{p,\mathrm{NL}}^2/\omega_{p,0}^2$, in the plane (r',z'), is shown at $z=52.5$ μm for $a_0=3$.

early. As can be seen from Figs. 1(b) and 1(c), there is a competing effect of the two quantities, in that both manifest spikes along the ridge of the wavefront. However, it is clear that the peaking of the density is much more pronounced than that of p_z, that is, of γ, thus leading to a stronger decrease of the phase velocity on axis than in the peripheral region of the wakefield. Figure 2 displays the surface plot of $\omega_{p,\mathrm{NL}}^2/\omega_{p,0}^2$, which indeed shows that the net effect is a decrease of the group velocity on axis.

A reconstruction of the first-order (azimuthal) induced magnetic field is carried out by integrating the nonhomogeneous extended wave equation for $B_{\theta,1}$, which in dimensional units reads

$$\Box^2 B_{\theta,1}-k_p^2\frac{n_0}{\gamma_0}B_{\theta,1}=-k_p\left(p_{z,0}\frac{\partial}{\partial r}+\frac{p_{r,1}}{v_g}\frac{\partial}{\partial\tau}\right)\frac{n_0}{\gamma_0}. \quad (34)$$

$B_{\theta,1}$ represents the dominant component of the induced quasistatic magnetic field in the wake behind the laser pulse. The numerical integration of Eq. (34) is preferable, although equivalent, to the numerical differentiation associated with

$$B_{\theta,1}=-\frac{1}{k_p}\left(\frac{\partial A_{z,0}}{\partial r}+\frac{1}{v_g}\frac{\partial A_{r,1}}{\partial\tau}\right).$$

Notice that the right-hand side of Eq. (34) can be derived, as a first-order quantity, from Eqs. (7) and (8), by introducing the comoving reference frame, the normalized variables, and the expansion of Eq. (16). In this connection, we notice that, due to the smallness of the parameter ϵ, the approximate equality $|\boldsymbol{B}_{\mathrm{laser}}|\approx(ck/\omega)\epsilon^{-1}|\boldsymbol{A}_{\perp,0}|$ shows that our model remains valid for $B_{\theta,1}\approx A_{\perp,0}$ in dimensionless units. This means that, as far as we are dealing with the relativistic amplitude of the laser, that is, $A\approx O(1)$, we can describe the generation of the azimuthal magnetic field as high as a fraction of a_0/ϵ, in the range of a few tens of megagauss, for $\epsilon=10^{-1}$.

In Fig. 3, the contour plots of the induced azimuthal magnetic field associated with the wakefield produced behind the laser pulse are shown, in the plane (r',z'), at $z=52.5$ μm (left column) and $z=316.1$ μm (right column), for $a_0=1$ [Fig. 3(a)] and $a_0=3$ [Fig. 3(b)]. At the lower intensity [Fig. 3(a), the structure of the magnetic field is such that at a given radial position, it changes sign along the z direction. This evidence is in contrast with the analytical results of [9–11] and with PIC simulations of [9,10,12–17]. Moreover, the periodicity of the magnetic wake is the same as that of the zeroth-order quantities displayed in Fig. 1. By increasing the laser intensity, as it occurs at later times [left frame of Fig. 1(a), or for $a_0=3$], the magnetic-field distributions manifest the formation of a background uniform component ($\approx$1 MG), with strong localized spikes ($\approx$ a few tens of MG) at the ridges of the wakefield. Therefore, this tubelike structure of the azimuthal magnetic field becomes more and more an intrinsic property of the wakefield [22] as the pulse intensity increases, due to the more powerful laser used, or because of the self-compression of the pulse itself during the propagation. Figure 4 shows the longitudinal [Fig. 4(a)] and the radial [Fig. 4(b)] profiles of the induced magnetic field in the case $a_0=3$. The almost uniform background field is well seen in [Fig. 4(a)]. If we estimate the electron Larmor radius of relativistic electrons with $p_z\approx 4$ [see Fig. 1(c)] as $\rho_L\approx c/\omega_{c,\mathrm{NL}}\approx\gamma c/\omega_{c,e}$, we get $\rho_L\approx 7$ μm for $B\approx 1$ MG and $\gamma\approx 4$, which is smaller than the typical transverse scale of the wake, estimated as $w_0=42.2$ μm. A main consequence of the presence of a strong magnetic field in the wake region is that any electron bunch loading from the outside of the accelerating wake will be strongly hampered. On the other side, this self-generated magnetic background field has a focusing polarity that can be exploited in order to achieve a better confinement of accelerated electrons [16]. However, either an externally applied magnetic field or the self-induced one can no longer be effective in confining the relativistic electrons due to the presence of periodic magnetic-field spikes of opposite polarity, with amplitude of the order of a few tens of MG.

As we have already pointed out, our model describes consistently the evolution of the laser pulse envelope during its interaction with the background plasma. The laser pulse is subjected to several deformations due to the nonlinear self-compression and the relativistic self-focusing. In Fig. 5, the time evolution of the longitudinal spatial distribution of the zeroth-order vector potential intensity (thick lines), taken on axis, is displayed for $a_0=1$ [Fig. 5(a)] and for $a_0=3$ [Fig. 5(b)]. In order to show the role of the electron density on the pulse shape dynamics, the density profiles are also shown (thin lines).

From Fig. 5, the difference is apparent between the on-axis profiles for the two cases $a_0=1$ [Fig. 5(a)] and $a_0=3$ [Fig. 5(b)]. It should be noticed that initially the evolution of the pulses in both cases is characterized by a syncronous self-compression and self-focusing, so that the ratio of the pulse length to its width is almost preserved, and the pulses maintain their initial proportions. In the $a_0=1$ case, the pulse peak is shifted back during its propagation, whereas in the $a_0=3$ case it is advanced relative to its initial position (in the comoving frame). The changes in the longitudinal profiles are also evident. The difference in the evolution of the

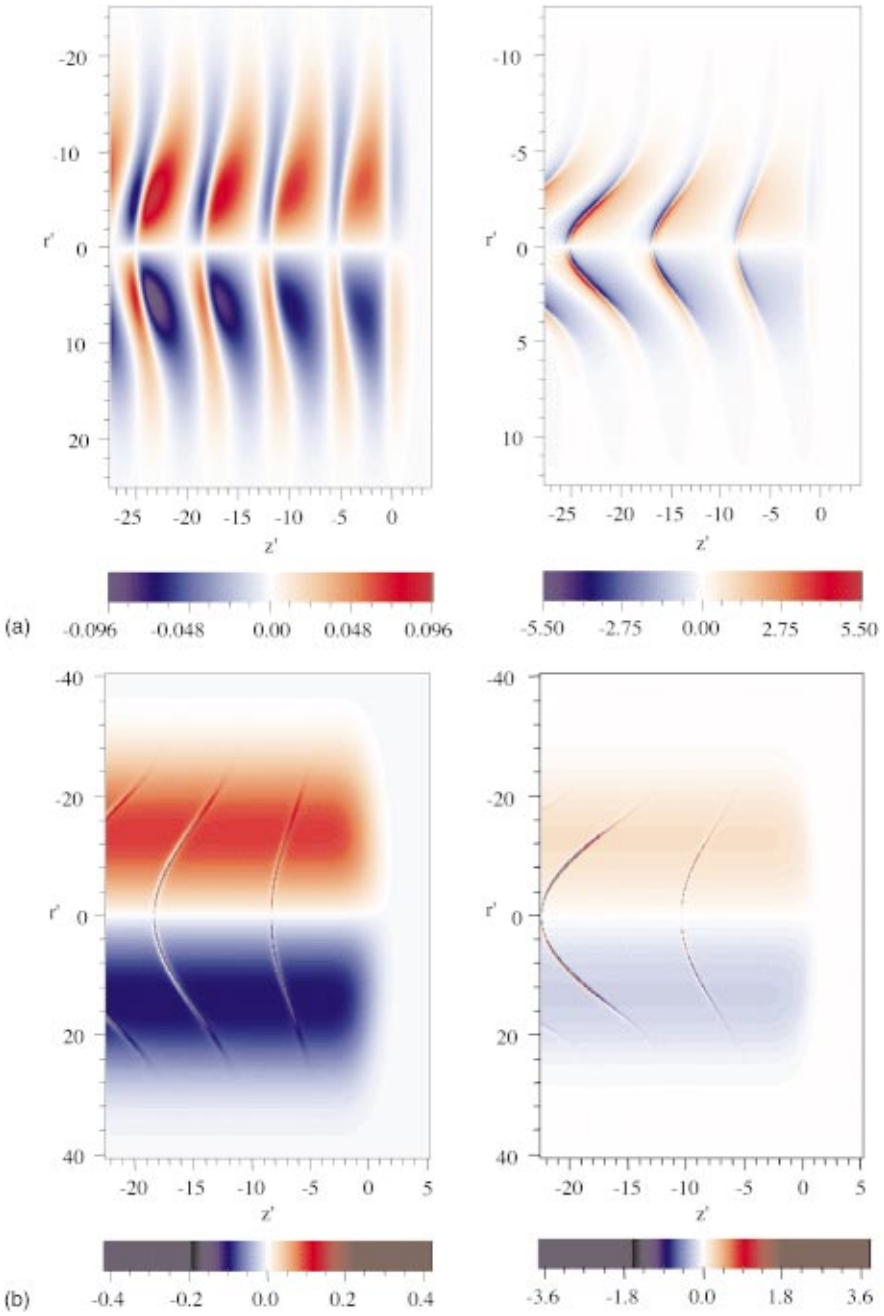

FIG. 3. (Color) The contour plots of the induced azimuthal magnetic field associated with the wakefield produced behind the laser pulse, in the plane (r',z'), at $z=52.5$ μm (left column) and $z=316.1$ μm (right column), for $a_0=1$ (a) and $a_0=3$ (b), are shown.

pulses reflects the complex interplay between the relativistic and the ponderomotive effects, which, contributing to the nonlinear refractive index, modify it in different ways. The relativistic mass increase of the electrons oscillating in the laser field depends on the magnitude of the laser intensity, while the ponderomotive force, which changes the electron density, depends on the magnitude of the gradient of the laser intensity. In both cases ($a_0=1$ and $a_0=3$), these gradients have the same order of magnitude. This is well seen in the density compression generated at the leading edge of both pulses: they have the same order of magnitude and similar profiles. At the same time, the intensity of the $a_0=3$ pulse is almost an order of magnitude higher than that of the $a_0=1$ pulse. Consequently, the modifications of the refractive index through the relativistic mass increase of electrons (hence the decrease in the local plasma frequency) in the $a_0=3$ case will be almost an order of magnitude higher than for the weaker pulse, resulting in the difference of the nonlinear refractive index, which eventually manifests itself in different propagation dynamics of the two pulses. We assign a thorough analysis of all the factors affecting the pulse evolution dynamics and the identification of the relevant physical mechanisms to a future work.

VI. CONCLUDING REMARKS

A physical model has been developed to investigate the interaction of ultrashort ($\ell_0 \ll \ell_\perp$) laser pulses with underdense plasmas. This model allows us to describe the laser pulse evolution and the generation of large wakefields self-

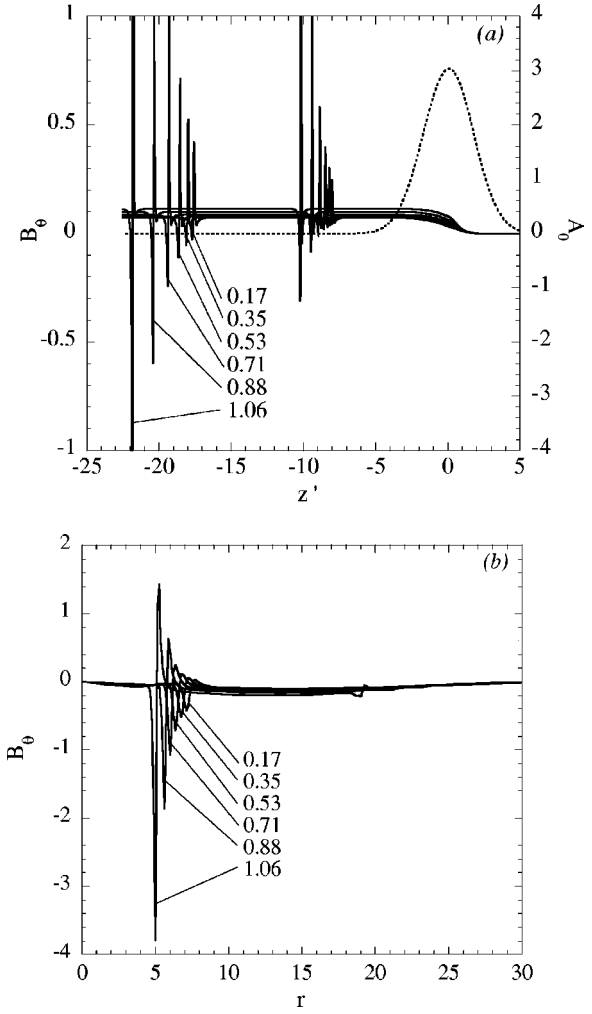

FIG. 4. The longitudinal (a) and the radial (b) profiles of the induced magnetic field (solid lines) are shown in the case $a_0=3$, taken at several times (indicated in the plots, in picoseconds) after the beginning of the interaction ($t=0$). The following correspondence between the instant of time and the pulse positions along the z axis, applies: 52.5 μm$\rightarrow$0.17 ps, 105.2 μm$\rightarrow$0.35 ps, 157.9 μm$\rightarrow$0.53 ps, 210.6 μm$\rightarrow$0.71 ps, 316.1 μm$\rightarrow$1.06 ps. The longitudinal profile of the vector potential amplitude, at $t=0$, is also displayed [dotted line, in (a)] for the sake of reference.

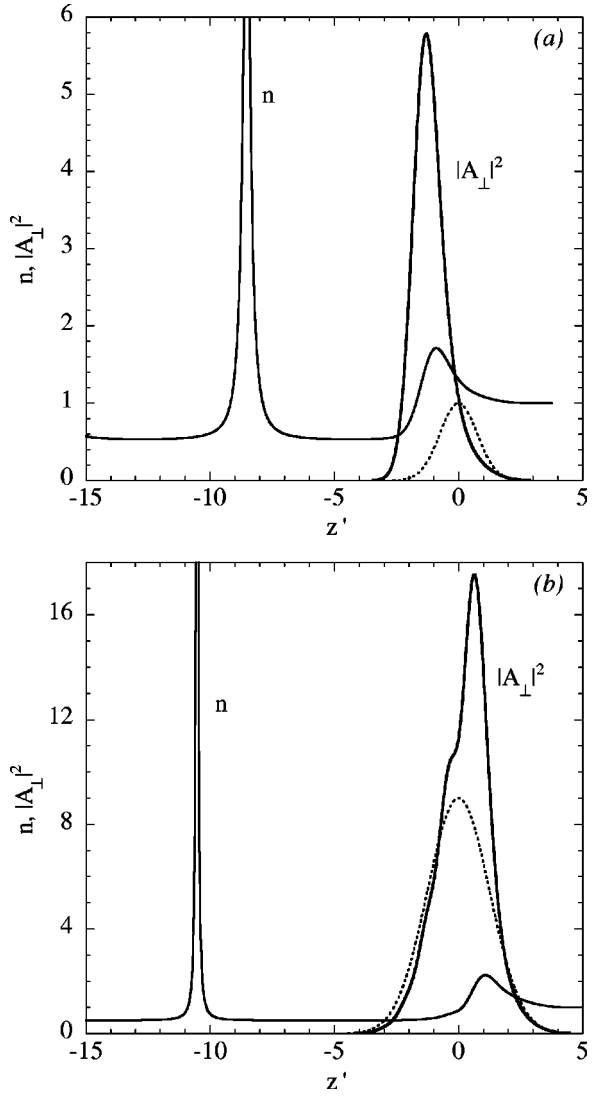

FIG. 5. The time evolution of the longitudinal spatial distribution of the zeroth-order vector potential intensity, taken on-axis, is displayed (thick full lines) at $t=2.21$ ps, corresponding to $z=658.7$ μm, for $a_0=1$ (a), and at $t=1.06$ ps, corresponding to $z=316.1$ μm, for $a_0=3$ (b). For the sake of comparison, the profiles at $t=0$ (dotted lines) are also shown. In order to show the role of the electron density on the pulse shape dynamics, the density profiles are also reported (thin lines).

consistently in a fully relativistic regime. Numerical studies of the problem are carried out using a developed multidimensional hydrodynamic code. The laser pulse evolution is described within the framework of the extended paraxial approach, retaining the cross space-time derivative along with the group velocity dispersion term. Taking into account all finite pulse length effects, our model is valid for ultrashort laser pulses down to a single-cycle regime. In an underdense plasma, the ''natural'' smallness parameter, $\epsilon=\omega_p/\omega<1$, allows one to write separate coupled equations for the magnetic field associated with the laser pulse, and for that pertaining to the quasistatic wakefield generated behind the pulse itself. This approach turns out to be very convenient in exploring the pulse-plasma interaction in the most favorable conditions for particle acceleration, where $E_z \gg E_\perp$. The code has been applied to two cases relative to two sub-20-fs pulses of $\approx$70 TW and $\approx$600 TW, respectively, and a wavelength of 1.06 μm, propagating in a strongly underdense plasma with an electron density of $\approx 10^{19}$ cm^{-3}. During the integration, the system has manifested a definitely nonstationary behavior: the laser pulse is compressed, self-focused, and, in the $a_0=3$ case, evenly split in two parts; consequently, the excited wakefield produces accelerating electric fields in the order of 0.5 TV/m, and density spikes up to 50 times the unperturbed density, values that are bounded even to increase during the subsequent evolution. The azimuthal magnetic field associated with the wakefield has been observed, which, at lower laser intensity, has a typical ring structure with neighboring rings that alternate in sign; however, with increasing pulse intensity, an almost uniform tube-

like background field is formed, on which periodical spikes appear, one order of magnitude more intense than the background field localized at the density distribution ridges.

The kinetic features, such as, for example, the electron acceleration due to wavebreaking, are not included within the model. This poses a limitation on its applicability, which, however, turns out to be not so severe in the case of strongly underdense plasmas ($\epsilon^2 \ll 1$). In this respect, we should notice that no sign of wavebreaking has been observed during the integrations that have been carried out.

Moreover, it is worth mentioning that if the field amplitude is not too large so as to excite a regular wakefield behind the pulse, it is expected that only a limited fraction of the laser energy is dissipated and transformed into an ''effective temperature'' of the plasma in the wakefield region. PIC simulations show that under these conditions, the highest electron energies are well below the electromagnetic energy inside the pulse and the corresponding typical velocities are appreciably smaller than the speed of light [23]. In this case, the cold hydrodynamic plasma model adopted here preserves most of the physics of the problem, as has also been shown by very recent comparisons between PIC and hydrodynamic simulations [24].

The backward Raman scattering process [25], which is known to affect heavily the pulse shape at small scales, is absent from our description. However, as far as the laser pulse remains shorter than the plasma wavelength $2\pi k_p^{-1}$, this process is not expected to play a dominant role [23].

As far as the intensities of the laser field and, consequently, of the quasistatic magnetic field are concerned, we are not restricted at all to weakly relativistic amplitudes. The fully relativistic regime of interaction, characterized by the normalized vector potential of the order of 1, can be accessed by our model, provided that the condition $B_{\theta,1} \approx A_{\perp,0}$ remains satisfied.

Finally, a comment on the possibility of diagnosing the quasistatic azimuthal magnetic field is in order. If we manage to use a linearly polarized probe laser propagating across the wakefield in such a way that it propagates tangent (that is, almost parallel) to the azimuthal field, the polarization rotation angle, for a path of 10 μm in a 1-MG ambient magnetic field, is of the order of 0.2°, a value that is within the present measurement capabilities.

The hydrodynamic code that has been used in these first simulations is particularly suitable for studying the multidimensional features of the ultrashort laser pulse interactions with underdense plasmas, namely the propagation of elliptical cross-section pulses, and the stability of azimuthal perturbations of the laser pulse, and the possible formations of filaments. This will be a matter of future investigations.

[1] G. Mourou and D. Umstadter, Phys. Fluids B **4**, 2315 (1992).
[2] M. D. Perry and G. Mourou, Science **64**, 917 (1994).
[3] G. Mourou, C. P. J. Barty, and M. D. Perry, Phys. Today **51** (1), 22 (1998).
[4] M. D. Perry, D. Pennington, B. C. Stuart, G. Tietbohl, J. A. Britten, C. Brown, S. Herman, B. Golick, M. Kartz, J. Miller, H. T. Powell, M. Vergino, and V. Yanovsky, Opt. Lett. **24**, 160 (1999).
[5] H. Wang, S. Backus, Z. Chang, R. Wagner, K. Kim, X. Wang, D. Umstadter, T. Lei, M. Murnane, and H. Kapteyn, J. Opt. Soc. Am. B **16**, 1790 (1999).
[6] K. Yamakawa, M. Aoyama, S. Matsuoka, T. Kase, Y. Akahane, and H. Takuma, Opt. Lett. **23**, 1468 (1998).
[7] E. Esarey, P. Sprangle, J. Krall, and A. Ting, IEEE Trans. Plasma Sci. **24**, 252 (1996).
[8] M. Tabak, J. Hammer, M. E. Glinsky, W. L. Kruer, S. C. Wilks, J. Woodworth, E. M. Campbell, and M. D. Perry, Phys. Plasmas **1**, 1626 (1994).
[9] L. Gorbunov, P. Mora, and T. M. Antonsen, Jr., Phys. Rev. Lett. **76**, 2495 (1996).
[10] L. Gorbunov, P. Mora, and T. M. Antonsen, Jr., Phys. Plasmas **4**, 4358 (1997).
[11] L. M. Gorbunov and R. R. Ramazashvili, J. Exp. Theor. Phys. **87**, 461 (1999).
[12] S. V. Bulanov, T. Zh. Esirkepov, M. Lontano, F. Pegoraro, and A. M. Pukhov, Phys. Scr. **T63**, 280 (1996).
[13] S. V. Bulanov, M. Lontano, T. Zh. Esirkepov, F. Pegoraro, and A. M. Pukhov, Phys. Rev. Lett. **76**, 3562 (1996).
[14] G. A. Askar'yan, S. V. Bulanov, G. I. Dudnikova, T. Zh. Esirkepov, M. Lontano, J. Meyer-ter-Vehn, F. Pegoraro, A. M. Pukhov, and V. A. Vshivkov, Plasma Phys. Controlled Fusion **39**, A137 (1997).
[15] G. A. Askar'yan, S. V. Bulanov, F. Califano, T. Zh. Esirkepov, M. Lontano, J. Meyer-ter-Vehn, N. M. Naumova, F. Pegoraro, A. M. Pukhov, and V. A. Vshivkov, Plasma Phys. Controlled Fusion **39**, B261 (1997).
[16] A. M. Pukhov and J. Meyer-ter-Vehn, Phys. Plasmas **5**, 1880 (1998).
[17] Z. M. Sheng, J. Meyer-ter-Vehn, and A. M. Pukhov, Phys. Plasmas **5**, 3764 (1998).
[18] E. Esarey, P. Sprangle, J. Krall, and A. Ting, IEEE J. Quantum Electron. **33**, 1879 (1997).
[19] B. Hafizi, A. Ting, P. Sprangle, and R. F. Hubbard, Phys. Rev. E **62**, 4120 (2000).
[20] V. I. Berezhiani and I. G. Murusidze, Phys. Lett. A **148**, 338 (1990).
[21] I. G. Murusidze and L. N. Tsintsadze, J. Plasma Phys. **48**, 391 (1992).
[22] A. G. Khachatryan, Phys. Plasmas **7**, 5252 (2000).
[23] S. V. Bulanov, I. N. Inovenkov, V. I. Kirsanov, N. M. Naumova, and A. S. Sakharov, Phys. Fluids B **4**, 1935 (1992).
[24] R. E. Giacone, J. R. Cary, B. A. Shadwick, E. Esarey, W. P. Leemans, D. Bruhwiler, P. Mardahl, and J. P. Verboncoeur, Bull. Am. Phys. Soc. **45**, 308 (2000).
[25] A. S. Sakharov and V. I. Kirsanov, Phys. Rev. E **49**, 3274 (1993).